Contents list available at IJRED website

International Journal of Renewable Energy Development

Journal homepage: https://ijred.undip.ac.id

Research Article

Prototype of a Solar Collector with the Recirculation of Nanofluids for a Convective Dryer

Denis del Sagrario García-Márquez, Isaac Andrade-González, Arturo Moisés Chávez-Rodríguez, Mayra I. Montero-Cortes, Vania Sbeyde Farías-Cervantes*

Postgraduate Studies and Research Division, Tecnológico Nacional de México Campus Tlajomulco, Km. 10 Carretera Tlajomulco-San Miguel, Tlajomulco de Zúñiga, C.P. 45640, Jalisco, México

Abstract. Solar collectors are thermal devices that can trap solar energy and convert it to heat. This heat can be used for different industrial applications, for example, the drying of food is one of the most useful applications of solar collectors. This work aims to design and build a solar collector using nanofluids for the convective drying of food. The dimensions of the solar collector were 1 m^2 by 20 cm with an angle of inclination of 45°. The collector was composed of 9-mm thick tempered glass and a heat exchanger in which the nanofluids circulate. Nanofluids were designed based on canola oil and nanopowders (>50 nm) of Al_2O_3, CuO, and a 1:1 (w/w) mixture of both. Thermal profiles were determined using differential scanning calorimetry (DSC). The solar collector temperatures were recorded using an Agricos® unit. The maximum temperatures of the air leaving the collector were 39.1°C, 44°C, 54°C, and 47.1°C for canola oil, and the nanofluids composed of Al_2O_3, CuO, and the 1:1 mixture, respectively, with a maximum efficiency of 65.09%. An increase in the outlet air temperature was observed using the nanofluids compared to canola oil alone

Keywords: Solar collector, Nanofluids, Solar radiation, Convective drying.

Received: 17th January 2022; Revised: 18th June 2022; Accepted: 20th July 2022; Available online: 18th August 2022

1. Introduction

Solar energy is a sustainable energy source that can be utilized for converting solar radiation to thermal energy. This transformation requires the use of photovoltaic cells or solar collectors, which capture the incident solar radiation and convert it to thermal energy (Besheer *et al.,* 2016). A recent study by Figueroa *et al.* (2021) showed that the use of solar energy in Tlajomulco de Zúñiga, Jalisco, Mexico is feasible due to its geographical situation and meteorological conditions. This is mainly due to the high level of solar radiation available, reaching maximum radiation peaks of 698.26 ± 85.84 W/m2, which could be used for different purposes.

For the capture and storage of this energy, solar collectors are widely used. Solar collectors are devices that absorb solar radiation and transfer heat to the absorbing fluid. The use of solar collectors has economic and environmental benefits; however, they must meet certain criteria, such as high system efficiency, low cost, useful life, useful reliability, low maintenance, and configuration flexibility of the system (Bangura *et al.,* 2022). Thermal efficiency is a crucial parameter that defines utility and cost, and therefore, a great deal of research focuses on improving the thermal performance of solar collectors. Solar collectors use three heat transfer mechanisms: conduction, convection, and radiation. Various types of solar thermal collectors exist, including concentrating (parabolic channel, heliostat, and parabolic dish) and non-concentrating (flat plate) collectors (Raj and Subudhi 2018). Currently, the use of solar thermal collectors is widespread because of their low cost and easy maintenance; however, the major drawbacks of solar thermal systems are intermittent solar radiation and lack of solar energy after sunshine hours. Hence, thermal energy storage plays a pivotal role in managing such radiation discontinuity (Mekahlia *et al.,* 2020; Senthil *et al.,* 2021). The collector most used at an industrial level is the flat plate collector, which is used for medium to high-temperature applications; however, it presents limited solar conversion efficiency and low operating temperatures (Eltaweel *et al.,* 2019). To counteract these problems, many researchers have modified this type of collector.

One of the suggested modifications is to replace regular working fluids with nanofluids because the transport fluids used in typical collectors lack efficient thermal and absorption properties. Shirole *et al.* (2021) reported that the dispersion of metallic or non-metallic solid particles in base fluids increased the heat storage and transfer efficiencies. The first particles studied were micrometer and millimeter sized; however, these sizes caused various problems such as rapid sedimentation of the particles and reduced pressure. Therefore, attention has shifted to the

* Corresponding author
Email: vaniasbeyde@gmail.com (V.S. Farías-Cervantes)

https://doi.org/10.14710/ijred.2022.44221
ISSN: 2252-4940/© 2022.The Author(s). Published by CBIORE

study of nanoparticles as the absorption media. For example, carbon-based nanofluids mixed with water showed broader absorption spectra and improved heat transfer coefficients by 33% to 40% with a concentration of 0.25 wt% for both turbulent and laminar flows (Amrollahi *et al.,* 2010; Gorji, 2017). Li *et al.* (2011) experimented using Al_2O_3, ZnO, and MgO and concluded that ZnO was most suitable for nanofluid applications in solar collectors. Vajjha and Das (2012), considered a mixture of water-ethylene glycol as fluid base fluid and dispersed nanoparticles of Al_2O_3, CuO, and SiO_2. Al_2O_3 nanofluid at 1% concentration showed a 31.9% increase in heat transfer coefficient. However, the study is useful only for the coldest regions. In general, the use of nanoparticles improves thermal stability due to the increased surface area, heat capacity, heat transfer rate, and convective heat transfer coefficient. The dispersion of nanofluids also ensures uniform temperature along the receiver's length, which reduces the temperature gradient and drives high thermal performance (Shirole *et al.,* 2021). Sun *et al.* (2017) examined the heat transfer characteristics of diverse types of nanofluids, such as copper, graphite, and aluminum, by using twisted tubes with external threads. Feizabadi *et al.* (2018), Khoshvaght-Aliabadi *et al.* (2016), Machrafi *et al.* (2016), and Khullar *et al.* (2012) investigated the effect of nanofluids (Al_2O_3) using different designs of tubes and flows in the collector. Although the incorporation of nanoparticles of some metals has been widely studied, various problems continue to arise, such as the stability of nanofluids, which is affected by the preparation technique, dispersion time, and the use of surfactants.

Most researchers have attempted to find solutions using water-based nanofluids. In this work, it is proposed to change the base fluid (water) to oil because heat transfer oils are commonly used for mid-range temperatures (100°C–400°C) and are more suitable for thermal cycles because oil has greater thermal stability. Choi *et al.* (2001) studied engine oil/carbon nanotube nanofluids and observed a 160% enhancement of thermal conductivity using 1 vol.% carbon nanotubes. Sokhansefat *et al.* (2014) numerically investigated the heat transfer enhancement for Al_2O_3/synthetic oil nanofluids in a parabolic trough collector tube. Their results showed that the heat transfer coefficient increased as the nanoparticle concentration in the base fluid increased. However, these investigations focused on the use of fossil and synthetic oils, which represent a high source of contamination. Furthermore, despite the extensive literature on different nanofluids, few studies refer to the application of vegetable oils. Canola oil is expected to achieve better dispersion, higher nanofluid stability in the collector, reduced sedimentation, lower pressure drop, as well as eliminate the need for surfactants because it possesses important thermal properties, such as viscosity and specific heat. Furthermore, it can potentially lead to reduced wear on the tubing used to recirculate the nanofluid, thus, improving the efficiency of the flat-layer collector. The objective of this work is to investigate the effects of nanofluids composed of different concentrations of Al_2O_3 and CuO nanoparticles in canola oil in a flat-layer solar collector.

2. Materials and Methods

2.1 Collector materials

The collector was equipped with a casing made of a 30-gage galvanized sheet painted matte black and PTR tubing (1 m * 22.5 cm). Fiberglass thermal insulation (2.5 cm thick) was used with a galvanized sheet absorber plate (1 m^2) painted matte black. The transparent cover was made of transparent tempered glass (1.05 m^2 * 9 mm thick). The solar collector was also equipped with a 0.5 in diameter copper tube heat exchanger consisting of 20 tubes, an air extractor consisting of an axial fan (mass flow = 3058.2166 m^3/h), a 20 L oil tank fully insulated with fiberglass (thickness = 2.5 cm), and a peripheral pump (power = 0.5 Hp) (Table 1, Figure 1). Figure 1 shows the solar collector coupled to a tray dryer prototype manufactured for this work.

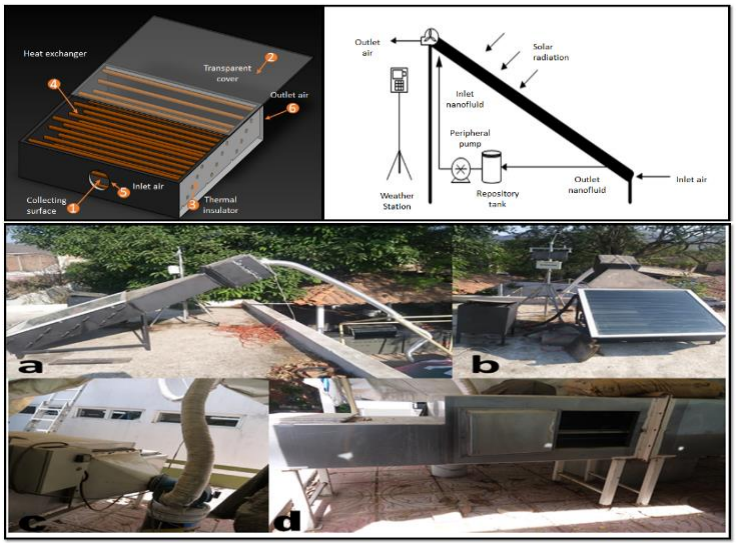

Fig. 1 Design of the solar collector with nanofluids coupled to a prototype tray dryer. a) Prototype placed on the roof of a room at an angle of 45°. b) Front view showing the components of the nanofluid recirculation tank, weather station, and solar collector. c) Connection of the collector to the tray dryer prototype through a pipe through which the air, previously heated by the solar collector with the nanofluid, flows. d) Prototype tray dryer

Table 1
Specifications of the flat plate solar collector

Specifications	Measurements
Area (absorption)	1.05 m²
Capacity of working fluid	20 L
Emissivity (absorber)	13%
Absorptivity (absorber)	97%
Material (absorber plate)	Copper
Transmissivity (glass)	80%
Thickness (glass)	9 mm
Number of tubes	20

2.2 Nanofluids

The nanofluids were prepared by mixing nanoparticles of aluminum oxide (Al_2O_3, molecular weight (MW) = 101.96 g/mol), copper oxide (CuO, MW = 79.55 g/mol), or a mixture (Al_2O_3:CuO (1:1 w/w)) in the base fluid consisting of canola oil at concentrations of 0.01wt%, 0.1wt%, and 0.5wt%.

2.3 Determination of the calorimetric profile of nanofluids

Differential scanning calorimetry (Linseis DSC, Model PT 1600, Germany) was used with calibration indium as the standard reference of the calorimeter. The samples were run in a temperature range of 20°C–400°C. The samples (4 mg) were placed in hermetically sealed aluminum volumetric crucibles. The experiments were carried out at a heating rate of 10°C/min. Data were analyzed using DSC software (Linseis TA).

2.4 Measurement of the temperature of the solar collector components

The solar collector tests were conducted in the pilot plant of the Technological Institute of Tlajomulco de Zúñiga, Jalisco, which is located within Tlajomulco de Zúñiga, Jalisco, Mexico (latitude (N): 20.44222; longitude (W): 103.4191667; altitude: 1566). The temperatures of the collecting surface and heat exchanger were measured using an infrared laser thermometer (STEREN® Model HER-425, China) during August and September 2019 on an 8 h schedule (00:00 am to 8:00 pm) at 30 min intervals. The environmental conditions (ambient temperature and incidence of solar radiation) varied significantly during the days sampled. The solar collector was placed facing south with an inclination angle of 35°.

2.5 Solar collector air temperature measurement

The manifold validation was performed using the three different types of nanofluids within the heat exchanger, as well as pure canola oil. The outlet air temperature was measured using a data acquisition module (AGRICOS®, Mexico). For each nanofluid used in the heat exchanger, the measurements were conducted over 7 days for 12 h periods. The evaluations were carried out from January to March 2020. The measurements were recorded in 5-min intervals for each of the following variables: temperature and relative humidity of the environment air, direction and air speed, temperature of the collector outlet air, relative humidity of the collector outlet air, temperature of the oil within the repository, and global solar radiation incident to the collector.

2.6 Thermal Efficiency

The thermal efficiency (η) of the solar system calculated by obtaining the ratio of useful energy gain to incident radiation, as shown in equation (1) (Charalambous *et al.*, 2007)

$$\eta = \frac{\dot{m}Cp(To-Ti)}{A_c G_t} \quad (1),$$

where $\dot{m}$ and Cp are the mass flow rate and heat capacity of the employed working fluid, respectively. Classical equations were used for the evaluation of the heat capacities of water and nanofluids (Kahani. 2019). Ac is the surface area of the solar collector and Gt is the global solar radiation.

2.7 Energy efficiency

The balanced equation of energy is given by equation (2).

$$\dot{Q}u = \dot{Q}abs - \dot{Q}loss \quad (2),$$

where $\dot{Q}u$ is the useful energy gain from $\dot{Q}abs$. $\dot{Q}$abs is the absorbed solar radiation with the extraction of $\dot{Q}loss$, which is the loss from convection, conduction, and radiation between the atmosphere and the collector. The loss can be calculated using equation (3).

$$\dot{Q}loss = U_L A_C (T_M - T_a) \quad (3),$$

where T_L is the overall heat transfer coefficient, A_C is the collector surface area, T_M is the mean plate temperature, and T_a is the ambient temperature. The overall heat transfer coefficient U_L was obtained from the detailed calculation conducted by Sakhaei and Valipour (2019).

There are issues with the use of T_M because the collector's temperature is not uniform throughout. Nevertheless, the heat removal factor (F_R) can be used to solve this problem. The heat removal factor was calculated using equation (4):

$$F_R = \dot{m}C_p(T_{out} - T_{in})/A_C\left(I_T(\tau\alpha) - U_L(T_{in} - T_{amb})\right) \quad (4)$$

where A_C is the collector area, C_p is the specific heat capacity of the fluid, T_{amb} is the ambient temperature, T_{in} is the working fluid inlet temperature, T_{out} is the working fluid outlet temperature, $\dot{m}$ is the mass flow rate, I_T is the total radiation, τ is the glass transmissivity, and α is the collector absorptivity.

The useful energy is given by equation 5:

$$\dot{Q} = A_C F_R\left(I_T(\tau\alpha) - U_L(T_{in} - T_{amb})\right) \quad (5),$$

The thermal efficiency of the collector is given by equation (6) (Eltaweel and Abdel-Rehim, 2020).

$$\eta = \dot{Q}/A_C I_T = F_R\left((\tau\alpha) - U_L(T_{in} - T_{amb})/I_T\right) \quad (6),$$

2.8 Drying kinetics

A tray dryer was used (provided by the LIDIA Analysis Company), and the solar collector was connected as shown in Figure 1 to supply the hot air and perform the kinetics analysis. The fruit to be dehydrated was banana with a 1 mm thickness per slice.

Table 2
Mathematical models used to fit the drying kinetics

Model Name	Model	Reference
Newton	$MR = \exp(-k * t)$	Vega *et al.* (2007)
Page	$MR = \exp(-k * t^n)$	
Henderson-Pabis	$MR = a * \exp(-k * t)$	Yagcioglu *et al.* (1999)
Wang-Singh	$MR = 1 + a * t + b * t^2$	Omolola *et al.* (2015)
Logarithmic	$MR = a * \exp(-k * t) + c$	Yaldiz and Ertekin (2001)

Drying was performed using hot air from the solar collector with an air speed of 2.56 m/s and a temperature of 40°C. Another experiment was carried out using a dryer with electric heating elements to heat the air. No previous treatment had been carried out on the fruit. Each of the experiments was performed in triplicate. The drying kinetics study using mathematical modeling allowed analysis of the drying behavior and characterization of the various foods (Lopez-Vidaña *et al.,* 2020). The values of the experimental moisture ratio versus the drying time were adjusted using five models widely used to model the drying kinetics of most foods (Table 2).

2.9 Determination of color

The color of the dehydrated banana slices was analyzed using objective measurements by direct reflection employing a colorimeter (X-rite®, United States). The instrument was calibrated using standard black and white tiles. Color differences were obtained using the "a," "b," and "L," parameters of the samples, where the "L," value indicates the darkness or lightness of the product, the "a," value indicates redness or greenness, and the "b," value indicates the yellowness or blueness of the sample (Farias *et al.,* 2016).

2.10 *Statistical analysis*

The coefficient of determination (R^2) and the root mean square error (RMSE) were used as the criterion of the goodness of fit of the experimental data against the data predicted by the mathematical models. A low value of chi-square indicates a better fit. The RMSE values provide information about the deviation of the experimental data against the predicted values, which are ideally close to 0. An R^2 value close to 1 indicates that there is a good fit of the data (Seerangurayar *et al.,* 2019; Lopez-Vidaña *et al.,* 2020).

3. Results dan Discussion

3.1 Solar collector component temperatures

Minimum and maximum incident radiations of 15 W/m^2 and 1141 W/m^2, respectively, and minimum and maximum ambient temperatures of 16.2°C of 28.5°C, respectively, were obtained. These results agree with those obtained by Figueroa *et al.* (2021). Figueroa *et al.* (2021) showed that this behavior could be explained by solar declination due to the position of the planet during its translation movement (Diez *et al.,* 2019), as well as the cloudiness throughout the year that causes changes in radiation in different months (Parreño *et al.,* 2020).

Table 3
Solar collector component temperatures

Room temperature	Incident Radiation	Capture surface	Heat exchanger	Side faces
16.2°C	15 W/m^2	15.7°C	14.4°C	14.1°C
28.5°C	1141 W/m^2	69.9°C	61.5°C	63.8°C

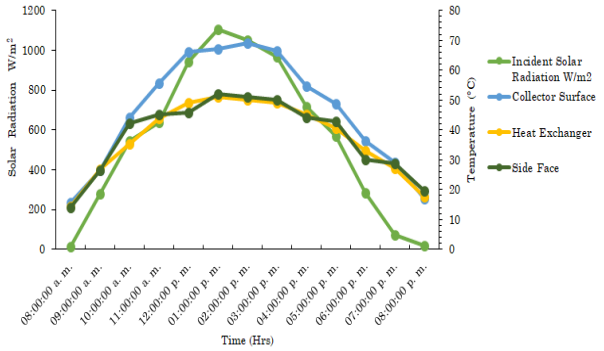

Fig. 2 Temperatures of the solar collector components with respect to the incident solar radiation

Table 3 shows the maximum and minimum temperatures of the components of the solar collector at ambient temperature and constant solar incidence, evaluated during the specified months. There were no significant temperature differences among the solar collector components. Figure 2 shows the temperature behavior of the different components on a single day in relation to the incident solar radiation. Once the incident solar radiation fell on the collector, the component temperatures began to rise and thus remained; even when the incident solar radiation began to decrease, the temperature of the components did not decrease quickly. The temperature decreased when the incident solar radiation on the solar collector was almost zero. This demonstrates the efficiency of the heat absorption of the materials used in the design of the solar collector. The heat exchanger temperature did not exceed 60°C because the temperature of copper cannot exceed this value. However, even with this temperature limitation, it was possible to dry the products with good quality. In comparison, Demou and Grigoriadis (2018) attained a temperature of 54°C with an incident solar radiation of 1141 W/m^2, which is lower than the maximum temperature of 63.8°C achieved in this work.

3.2 Thermal efficiency

The solar collector thermal efficiencies using different nanofluids are shown in Table 4 and Figure 3. The peak thermal efficiency was 65.09% and the average efficiency was about 48.99% with variations in the solar radiation from 15 to 1141 W/m^2. The nanofluid consisting of CuO and canola oil presented the highest thermal efficiency. This may be because CuO presented fewer sedimentation problems and allowed higher flow rates during recirculation. The collision between particles helped to extract heat from the collector pipe, which appeared as a rise in the efficiency. Since the design of the collector (*i.e.*, the collector size, the materials used, and the experimental location) affects the performance, all of these factors affected the experiment and changed the results each time. Therefore, changes were observed in the efficiency yields of the solar collectors, thus providing guidelines for further investigation.

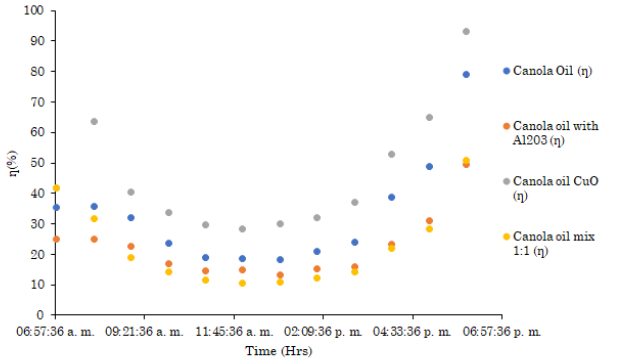

Fig. 3 Thermal efficiencies of the solar collector with the use of nanofluids throughout the day

These results were similar to those reported by Lopez-Vidaña *et al.* (2020) and Sadeghzadeh *et al.* (2019). However, when the solar irradiance decreased at the end of the day, the efficiencies increased considerably**,** as shown in Figure 3.

3.3 Energy efficiency

Table 4 shows the energy efficiencies of the solar collector using the different nanofluids. The highest efficiency was achieved using canola oil with 0.1% CuO. The increase in efficiency seemed to be due to the reduced heat loss and better retention achieved using this nanofluid. This behavior may be due to the relatively high thermal conductivity and low specific heat of the 0.1% CuO nanofluid (the influence of increased conductivity and lower specific heat can be understood in terms of a higher temperature gradient). Furthermore, the greater temperature difference between the nanofluid inlet and outlet in the solar collector occurred because the collision between the nanoparticles was intensified. Therefore, a greater microconvection was present, which appeared as a greater thermal efficiency. Utilizing the optimum quantity of nanoparticles maximized the benefits of harnessing solar energy from the thermal collector (Choudhary *et al.*, 2021). Similar results were found by Choudhary *et al.* (2020), although improved energy efficiencies were achieved in this work.

3.4 Nanofluids

In the present work, different concentrations of nanoparticles suspended in the base fluid (canola oil) were tested. Figure 4 shows the behavior of the different nanofluid concentrations (0.01%, 0.1%, and 0.5%) of Al_2O_3, CuO, and the Al_2O_3: CuO (1:1) mixture.

Table 4
Thermal efficiencies of the solar collector using different nanofluids

Nanofluid	Thermal efficiency (%)	Energy efficiency (%)
Canola oil	30.33	76.52
Canola oil + Al_2O_3 0.1%	49.63	85.09
Canola oil + CuO 0.1%	65.09	90.89
Canola oil + Mix (1:1)	50.91	64.06

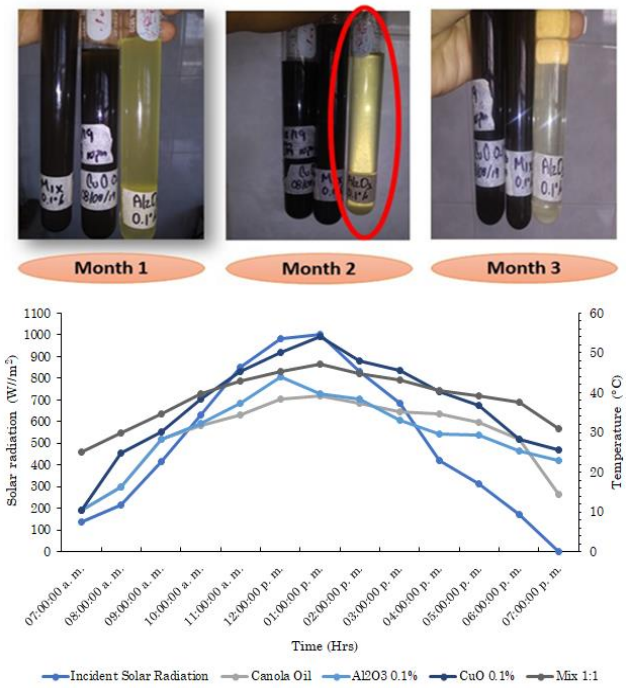

Fig. 4 Sedimentation of the nanoparticles in the different nanofluids after different periods of rest. Temperatures of the nanofluids reached as a function of the incident solar radiation throughout the day

Typically, as the nanoparticle concentration increases, the ability of the nanofluid to absorb solar radiation increases; however, this behavior was not observed in this work. After three months at rest, the nanofluids that showed the lowest sedimentation were 0.1% CuO and the Al_2O_3: CuO mixture. This is because there are limitations to the nanoparticle concentration, which should not exceed 0.5% by weight to avoid such problems as sedimentation and high pressure drop (Paul *et al.,* 2010). The Al_2O_3 nanoparticles presented greater sedimentation in all concentrations, corresponding to the work of Lee and Mudawar (2007) who found that high concentrations, nanoparticle sizes, and Van der Waals forces were responsible for sedimentation.

3.5 Calorimetric profile of nanofluids

Figure 5 shows the thermograms of the different nanofluids (CuO, Al_2O_3, and Al_2O_3: CuO (1:1) mixture) at a concentration of 0.1%. For all the nanofluids, the 0.1% concentration presented the longest stabilization time before sedimentation occurred, using pure canola oil as the control. For the nanofluids, the smoking point started at 315°C, which was delayed compared to canola oil, for which the smoking point began at 175°C. Therefore, the oxidation process began at 220°C for canola oil and 425°C for the nanofluids. This is naturally attributed to the volatilization and combustion of triglycerides, however, with the addition of the nanoparticles, the conductivity and thermal stability increased because the random collision of nanoparticles increased with the increase in concentration. Thus, microconvection becomes dominant in heat transfer, which enhances thermal conductivity (Bahiraei and Hangi 2016). The degradation process of canola oil began at 175°C.

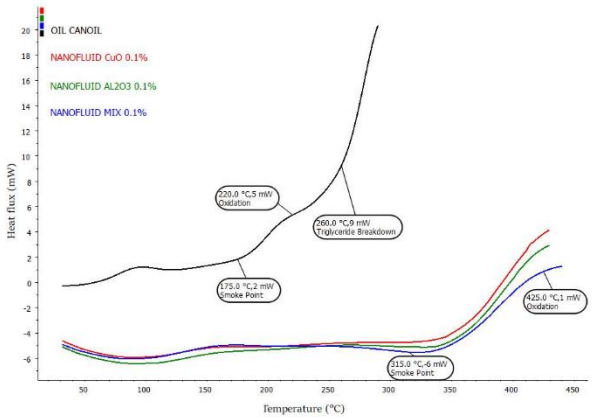

Fig. 5 Smoke point thermogram of nanofluids versus canola oil

The next change occurred at 220°C (a difference of 45°C), with the complete destruction of triglycerides occurring at 260°C. In contrast, the first reaction for the nanofluids was observed at 315°C, with the second change occurring at 425°C. Thus, there was a difference of 110°C between canola oil and the nanofluids. The thermograms demonstrate that the nanofluids did not reach a state of irreversible decomposition at 400°C, unlike canola oil, which reached a state of structural change at 260°C.

3.6 Solar collector outlet air temperature measurement

Table 5 presents the air temperatures reached using the different working fluids inside the heat exchanger. The ambient temperatures or initial temperatures in the collector were similar for the four working fluids. Considerable differences were observed in the outlet air temperatures with the use of different working fluids. For the canola oil and CuO nanofluid, the outlet air temperature inside the heat exchanger reached 54°C, which was higher than the temperatures reached using the other fluids. The outlet air temperatures recorded using the other nanofluids were similar, with a difference of 3°C. These values were higher than the value of 46°C reported by Hajar *et al*. (2017). The thermal efficiency of nanofluids depends on different attributes (*i.e.*, types of nanoparticles, base fluid, thermophysical properties, *etc*.), which directly or indirectly affect the nanofluid performance in different applications (Sandhu *et al*., 2016). However, the temperature difference observed here was more likely due to Brownian motion and convection of the CuO nanoparticles at a concentration of 0.1% in the base fluid (canola oil).

Table 5
Manifold outlet air temperatures using different working fluids

Work flow	Maximum radiation reached (W/m$^{2)}$	Maximum ambient air temperature (°C)	Manifold outlet air temperature (°C)
Canola oil	827	23.4	39.1
Nanofluid canola oíl and Al_2O_3	743	24.4	44.1
Nanofluid canola oil and CuO	961	27	54
Nanofluid canola oil an 1:1 blend	1000	31.2	47.1

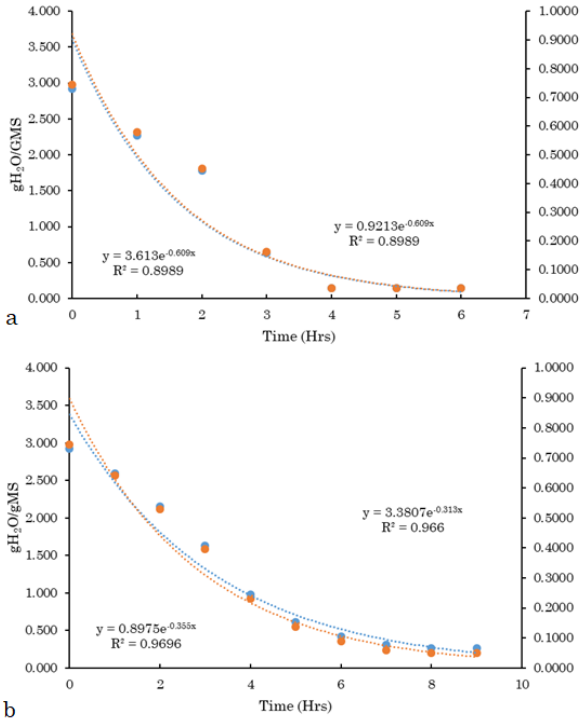

Fig. 6 Drying kinetics using a) a tray dryer with electrical resistance and b) a tray dryer with a solar collector and nanofluids

Table 6
Values of the drying constants and coefficients of different models determined through regression method.

Models	Parameter	Dryer Type	
		Dryer with solar collector with nanofluids	Electric tray dryer
Newton	k	0.293527	0.313705
	R^2	0.9467	0.9564
	SSE	0.174672	0.104024
	RMSE	0.0116448	0.0080018
Page	k	0.09032	0.13558
	n	1.91232	1.70558
	R^2	0.998	0.996
	SSE	0.0063388	0.0062475
	RMSE	0.0005282	0.0006248
Henderson and Pabis	k	0.32156	0.3378
	a	1.10198	1.07688
	R^2	0.937	0.951
	SSE	0.144484	0.0877563
	RMSE	0.0103203	0.007313
Wang and Singh	a	-0.193448	-0.212897
	b	0.006472	0.008185
	c	0.982	0.988
	R^2	0.0410714	0.021728
	SSE	0.0029337	0.0018107
	RMSE		
Logarithmic	k	0.10645	0.11299
	a	2.06852	2.06162
	c	-1.02258	-1.03289
	R^2	0.982	0.986
	SSE	0.0376923	0.0211527
	RMSE	0.0028994	0.001923

Table 7
Cost comparison of electric tray dryer versus nanofluid-based solar collector dryer

Dryer type	Dryer preheating cost	Watts	Current (A)	Total cost of drying
Electric tray dryer	$8.65	9583.09	20.76	$112.49
Dryer with solar collector with nanofluids	$16.55	0	0	$98.98
Dryer with solar collector without nanofluids	$22.68	0	0	$108.67

3.7. Dying kinetics with the heat exchanger

Figure 6 shows the drying kinetics using an electric tray dryer versus a tray dryer using a solar collector and nanofluids. The drying times to achieve a moisture content below 10%, the moisture content necessary for the banana slices to remain stable, were 3.5 h with the electric tray dryer and 6 h with the dryer using the solar collector with nanofluids. The operating conditions (temperature, airflow, and the number of banana slices) in both dryers were the same. The increase in drying time using the solar collector with nanofluids may be because the food in the lower levels absorbed the energy of the hot air coming from the solar collector and the air interchanged energy with the banana slices; thus, decreasing the temperature and consequently the drying potential of the banana slices. This may also be due to the unstable behavior of the temperature inside the drying chamber because the drying chamber was constantly being opened to weigh the samples.

For the modeling of the drying curves, the Newton, Page, Henderson–Pabis, Wang–Singh, and logarithmic models showed R^2 values between 0.94 and 0.99 for the temperatures and operating conditions evaluated in both dryers (Table 6). Comparing the R^2 and RMSE values of all the models, the Page model presented the best fit to the experimental data (parameters shown in Table 6) because it presented the highest R^2 and the lowest RMSE values. Conversely, the Henderson–Pabis and Newton models showed the worst fits based on their low R^2 values and high RMSE values. It was concluded that the Page model was more useful in estimating the drying kinetics of banana slices under all drying temperatures due to its lean mathematical form. Similarly, the Page model was found to be the most appropriate model in various other studies (Başlar *et al.*, 2015; Martins *et al.*, 2015; Kılıç, 2017; Aykın-Dinçer and Erbaş, 2019). Majdi (2018) experimented with different air flows to dry apples and found that the best results in terms of product quality and reduction of energy costs were achieved by drying with a greater airflow (speed of 5 m/s) using solar energy. This agrees with the results of this study in which the dehydrated product quality achieved using solar energy was better than that using the dryer with electrical resistance.

Table 7 shows the costs of each of the dryers used in the drying of the banana slices. The lowest total drying cost was achieved using the dryer with the solar collector and nanofluids ($98.98), regardless of the longer drying times. Furthermore, the cost of using the solar collector without nanofluids was higher than the cost with nanofluids. Therefore, the use of a solar collector with nanofluids has a wide potential for fruit drying.

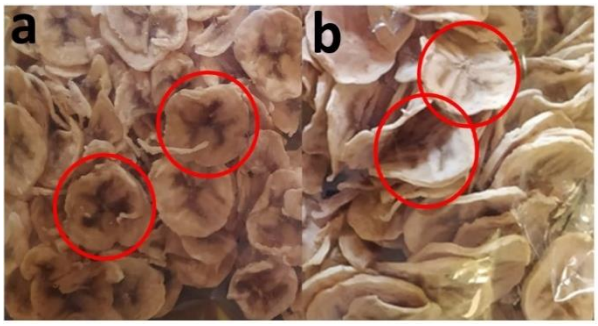

Fig. 7 Final product using two different types of drying: a) product dried with electrical resistance and b) product dried with the solar collector

Table 8
Comparison of the color parameters obtained from banana slices dehydrated in a dryer with electrical resistance and a dryer with a solar collector and nanofluids

Dryer type	L	*a	*b
Electric tray dryer	46.30±2.44[b]	15.11±2.80[a]	19.91±1.69[a]
Dryer with solar collector with nanofluids	69.10±4.17[a]	8.29±4.56[b]	15.09±6.33[a]

3.8. Color

The color specification of a food product is simply the specification of a point in three-dimensional space, in which the visual or mathematical expression of color has become known as a color solid (Waliszewsk *et al.,* 2007). The color determination results are shown in Figure 7 and Table 8. Significant differences can be observed between the dehydrated banana slices obtained using the dryer with electrical resistance and the dryer with a solar collector and nanofluids. The L value decreased when using the dryer with electrical resistance. This is because the color changed from pale yellow to a more intense dark yellow, indicating a decrease in the L value. This behavior is also reflected in the increase in the value of a, indicating more browning; therefore, the use of the solar collector with nanofluids prevented the browning of the banana slices. Similar results were reported by Tabtiang *et al.* (2011).

4. Conclusion

The methodology applied in the design allowed the construction and operation of a flexible solar collector for use under different operating conditions. The prototype was designed to provide heat from a sustainable energy source and avoid the consumption of polluting and highly expensive energy sources. It was possible to obtain hot air by transforming solar radiation into thermal energy and to carry out drying processes with reduced costs. Nanofluids lose heat over a shorter time than canola oil. The use of nanofluids inside the heat exchanger contributed to an increase in the outlet air temperature, with temperatures of 39.1°C, 44°C, 54°C, and 47.1°C achieved using canola oil and nanofluids composed of Al_2O_3, CuO, and a Al_2O_3: CuO (1:1) mixture, respectively, at concentrations of 0.1 vol.%. Of the three nanofluids, the nanofluid with CuO reached the highest temperature. However, an outlet air temperature of 80°C was not achieved, possibly due to the design of the collector in which the heat exchanger had large spaces between the tubes. As a result, only the contact surface area of the air entering the solar collector was heated, rather than the entire volume of air. However, the thermal efficiencies were comparable to those of other investigations, thus demonstrating the potential for using the canola oil and CuO (0.1%) nanofluid in a solar collector. Furthermore, the design of the collector allows easy disassembly and transportation, thus the solar collector can be used as a heat source for different processes or different convective dryers.

Acknowledgments

We are grateful for the support of the National Council of Science and Technology (CONACYT for its acronym in Spanish) for the scholarship granted to study the Master of Science in Agrobiotechnology of the program of the National Technology of Mexico campus Tlajomulco included in the standard of excellence for graduates. The authors would like to thank Enago (www.enago.com) for the English language review.

Author Contributions: Denis del Sagrario García-Márquez; experimental development in the field, Isaac Andrade-González; conceptualization, methodology, formal analysis, Arturo Moises Chávez-Rodríguez; writing—review and editing, project administration, validation, Mayra I. Montero-Cortes; writing—review and editing, Vania Sbeyde Farias-Cervantes; writing—review and editing, project administration, validation. All authors have read and agreed to the published version of the manuscript.

Funding: This research had no funding

Conflicts of Interest: The authors declare no conflict of interest.

References

Aykın-Dinçer, E., Erbaş, M. (2019). Cold dryer as novel process for producing a minimally processed and dried meat. *Innovative Food Science & Emerging Technologys* 57, 102113. https://doi.org/10.1016/j.ifset.2019.01.006

Amrollahi, A., Rashidi, A.M., Lotfi, R., Meibodi, M.E. & Kashefi, K. (2010). Convection heat transfer of functionalized MWNT in aqueous fluids in laminar and turbulent flow at the entrance region. *International Communications in Heat and Mass Transfer* 37, 717-723. https://doi.org/10.1016/j.icheatmasstransfer.2010.03.003

Bahiraei, M. & Hangi, M. (2016). Investigating the Effect of Line Dipole Magnetic Field on Hydrothermal Characteristics of a Temperature-Sensitive Magnetic Nanofluid Using Two-Phase Simulation. *Nanoscale Research Letters* 11, 443. https://doi.org/10.1186/s11671-016-1661-9

Başlar, M., Kilicli, M., Yalinkilic, B. (2015). Dehydration kinetics of salmon and trout fillets using ultrasonic vacuum drying as a novel technique. *Ultrasonics Sonochemistry* 27, 495–502. https://doi.org/10.1016/j.ultsonch.2015.06.018

Bangura, A.B.M., Hantoro, R., Fudhloli, A., Uwitije, P.D. (2022) Mathematical Model of the Thermal Performance of Double-pass Solar Collector for Solar Energy Application in Sierra Leone. *Int. J. Renew. Energy Dev*, 11(2), 347-355 https://doi.org/10.14710/ijred.2022.41349

Besheer A.H., Smyth, M., Zacharopoulos, A., Mondol, J. & Pugsley, A. (2016). Review on recent approaches for hybrid PV/T solar technology. *International Journal of Energy Research* 40(15), 2038-2053. https://doi.org/10.1155/2012/307287

Bourriot, S., Garnier, C. & Doublier, J.L. (1999). Phase separation, rheology and microstructure of micellar casein-guar gum

mixtures. *Food Hydrocolloids* 7, 90-95. https://doi.org/10.1016/S0268-005X(98)00068-X

Castillo-Téllez, M., Pilatowsky-Figueroa, I., López-Vidaña, E.C., Sarracino-Martínez, O. & Hernández, G. (2016). Dehydration of the red chilli (*Capsicum annuum* L., costeño) using an indirect-type forced convection solar dryer. *Applied Thermal Engineering,* 114(5), 1137-1147. https://doi.org/10.1016/j.applthermaleng.2016.08.114

Choi, S.U.S, Zhang, Z.G., Yu. W., Lockwood. F.E., Grulke. E.A. (2001). Anomalous thermal conductivity enhancement in nanotube suspensions. *Applied Physics Letters*, 79(14), 2252–4. https://doi.org/10.1063/1.1408272

Choudhary, S., Sachdeva, A., & Kumar P. (2021): Time-based assessment of thermal performance of flat plate solar collector using magnesium oxide nanofluid. *International Journal of Sustainable Energy*, 40(5), 460-476. https://doi.org/10.1080/14786451.2020.1814288

Demou, D. & Grigoriadis, D.G.E. (2018). 1D model for the energy yield calculation of natural convection solar air collectors, *Renewable Energy*, 119, 649–661. https://doi.org/10.1016/j.renene.2017.12.030

Diez, F.J., Navas-Gracia, L.M., Martínez-Rodríguez, A., Correa-Guimaraes, A. & Chico- Santamarta, L. (2019). Modelling of a flat-plate solar collector using artificial neural networks for different working fluid (water) flow rates. *Solar Energy* 188, 1320-1331. https://doi.org/10.1080/01430750.2018.1525576

Eltaweel, M., Ahmed A. Abdel-Rehim & Hussien, H. (2019). Indirect thermosiphon flat-plate solar collector performance based on twisted tube design heat exchanger filled with nanofluid. *Energy Research* 44(6), 4269-4278. https://doi.org/10.1002/er.5146

Farias-Cervantes, V., Delgado-Licon, E., Solís-Soto, A., Medrano-Roldan, H. & Andrade-González, I. 2016. Effect of Spray Drying Temperature and Agave Fructans Concentration as Carrier Agent on the Quality Properties of Blackberry Powder. *International Journal of Food Engineering* 5(12), 451–459. https://doi.org/10.1515/ijfe-2015-0287

Feizabadi, A., Khoshvaght-Aliabadi, M. & Rahimi, A.B. (2018). Numerical investigation on Al2O3/water nanofluid flow through twisted serpentine tube with empirical validation. *Applied Thermal Engineering* 137, 296-309. https://doi.org/10.1016/j.applthermaleng.2018.03.076

Figueroa-Garcia, E. Segura-Castruita, M.A., Luna-Olea, F.M., Vázquez-Vuelvas, O.F. & Chávez-Rodríguez, A.M. (2021). Design of a hybrid solar collector with a flat plate solar collector and induction heating: evaluation and modelling with principal components regression. *Revista Mexicana de Ingeniería Química* 20(3), 1-14. https://doi.org/10.24275/rmiq/Alim2452

Gorji, T.B. & Ranjbar, A. (2017). Thermal and exergy optimization of a nanofluid-based direct absorption solar collector. *Renew Energy* 106, 274-287. https://doi.org/10.1016/j.renene.2017.01.031

Hajar, E., Rachid, T. & Najib, B.M. (2017). Conception of a solar air collector for an indirect solar dryer. *Pear drying test, Energy Procedia* 141, 29-33. https://doi.org/10.1016/j.egypro.2017.11.114

Kasaeian. A.B., Sokhansefat, T., Abbaspour, M.J., Sokhansefat, M. (2012) Numerical study of heat transfer enhancementby using Al_2O_3/synthetic oil nanofluid in aparabolic trough collector tube. *Rome: World Academy of Science, Engineering and Technology*, 1154–9.

Khoshvaght-Aliabadi, M. & Arani-Lahtari, Z. (2016). Forced convection in twisted minichannel (TMC) with different cross section shapes: a numerical study. *Applied Thermal Engineering* 93, 101-112. http://dx.doi.org/10.1016/j.applthermaleng.2015.09.010

Khullar, V., Tyagi, H., Phelan PE, Otanicar, T.P., Singh, H. & Taylor, R.A. (2012). Solar energy harvesting using Nanofluids-based concentrating solar collector. *Journal of Nanotechnology in Engineering and Medicine* 3 (3), 031003 (9). https://doi.org/10.1115/1.4007387.

Kiliç, A. (2017). LTHV (Low Temperature and High Velocity) drying characteristics and mathematical modeling of anchovy (Engraulis encrasicolus). *GIDA* 42(6), 654–665. https://doi.10.15237/gida.GD17043.

Lee, J., Mudawar, I. (2007). Assessment of the effectiveness of nanofluids for single-phase and two-phase heat transfer in micro-channels. *International Journal of Heat and Mass Transfer* 50(3), 452-463. https://doi.org/10.1016/j.ijheatmasstransfer.2006.08.001

Li, N., Taylor, L.S., & Mauer, L.J. (2011). Degradation kinetics of catechins in green tea powder: Effects of temperature and relative humidity. *Journal of Agriculture and Food Chemistry*, 59, 6082–6090. https://doi.org/10.1021/jf200203n

López-Vidaña, E. C., Cesar-Munguía, A. L., García-Valladares, O., Pilatowsky, I., and Brito-Orosco, R. (2020). Thermal performance of a passive, mixed-type solar dryer for tomato slices (Solanum lycopersicum). *Renewable Energy* 147, 845-855. https://doi.org/10.1016/j.renene.2019.09.018

Machrafi, H., Lebon, G. & Iorio, C.S. (2016). Effect of volume-fraction dependent agglomeration of nanoparticles on the thermal conductivity of nanocomposites: applications to epoxy resins, filled by SiO_2, AlN and MgO nanoparticles. *Composites Science and Technology* 130, 78-87. https://doi.org/10.1016/j.compscitech.2016.05.003.

Majdi, J.E. (2018). Optimization of convective drying by response sufance methodoly *Computers and Electtronics in Agriculture* 156, 574-584, https://doi.org/10.1016/j.compag.2018.12.021

Martins, M.G., Martins, D.E.G., Pena, R.D.S. (2015). Drying kinetics and hygroscopic behavior of pirarucu (Arapaima gigas) fillet with different salt contents. *LWT – Food Science Technology* 62(1), 144–151. https://doi.org/10.1016/j.lwt.2015.01.010

Mekahlia, A., Boumaraf, L. & Abid, Ch. (2020). CFD analysis of the thermal losses on the upper part of a flat solar collector. *Heat Transfer* 11(2), 99-112. https://doi.org/10.29019/enfoque.v11n2.601

Mohandes, N., Sanfilippo, A. & Al Fakhri, M. (2019). Modeling residential adoption of solar energy in the Arabian Gulf Region. *Renewable Energy* 131, 381-389. https://doi.org/10.1016/j.renene.2018.07.048

Omolola, A.O., Jideani, A.I.O. and Kapila, P.F. 2015. Drying Kinetics of Banana (Musa Spp.). *Interciencia*, 40, 374-380. https://www.interciencia.net/wp.

Parreño, J., Lara, O., Jumbo, R., Caicedo, H. & Sarzosa, D. (2020). Diseño de un módulo de energía solar como estrategia de ahorro energético y disminución de la emisión de CO2. *Agroindustria, Sociedad y Ambiente* 2(15), 4-18. https://revistas.uclave.org/index.php/asa/article/view/2849

Paul, G., Chopkar, M., Manna, I. & Das, P.K. (2010). Techniques for measuring the thermal conductivity of nanofluids: a review. *Renewable and Sustainable Energy Reviews* 14, 1913-1924. https://doi.org/10.1016/j.rser.2010.03.017

Raj, P. & Subudhi, S. (2018). A review of studies using nanofluids in flat plates and direct solar absorption. *Renewable and Sustainable Energy Reviews* 84, 54-74. https://doi.org/10.1016/j.rser.2017.10.012.

Sadeghzadeh, M., Ahmadi, M.H., Kahani, M., Sakhaeinia, H., Chaji, H., Chen, L. (2019). Smart modeling by using artificial intelligent techniques on thermal performance of flat-plate solar collector using nanofluid. *Energy Science & Engeniering* 7(5), 1649-1658. https://doi.org/10.1002/ese3.381

Sandhua, H., Gangacharyulua, D. & Agrawal, V.P. (2016). Coding, evaluation, comparison, ranking and optimal selection of nanoparticles with heat transfer fluids for thermal systems. *Particulate Science and Technology* 36(1), 50-60. https://doi.org/10.1080/02726351.2016.1208695

Seerangurayar, T., Al-Ismaili, A. M., Janitha Jeewantha, L. H., Al-Nabhani, A. 2019. Experimental investigation of shrinkage and microstructural properties of date fruits at three solar drying methods. *Solar Energy* 180, 445-455. January. https://doi.org/10.1016/j.solener.2019.01.047

Senthil, R., Priya, I.I.M., Gupta, M., Rath, C., Ghosh, N. (2021) Experimental Study on Solar Heat Battery using Phase Change Materials for Parabolic Dish Collector. *International Journal of Renewable Energy Development*, 10(4), 819-825. https://doi.org/10.14710/ijred.2021.38376

Shirole A, Wagh, M, Kulkarni V. (2021) Thermal Performance Comparison of Parabolic Trough Collector (PTC) Using Various Nanofluids. *International Journal of Renewable*

Energy Development, 10(4), 875-889 https://doi.org/10.14710/ijred.2021.33801

Sun, B., Yang, A. & Yang, D. (2017). Experimental study on the heat transfer and flow characteristics of nanofluids in the built-in twisted belt external thread tubes. *International Journal of Heat and Mass Transfer* 107, 712-722. https://doi.org/10.1016/j.ijheatmasstransfer.2016.11.084

Tabtiang, S., Prachayawarakon, S. & Soponronnarit, S. (2012) Effects of Osmotic Treatment and Superheated Steam Puffing Temperature on Drying Characteristics and Texture Properties of Banana Slices. *Drying Technology: An International Journal* 30(1), 20-28. http://dx.doi.org/10.1080/07373937.2011.613554

Vajjha, R. S., and D. K. Das. 2012. A review and analysis on influence of temperature and concentration of nanofluids on thermophysical properties, heat transfer and pumping power. *International Journal of Heat and Mass Transfer* 55, 4063–78. https://doi:10.1016/j.ijheatmasstransfer.2012.03.048

Vega, a. P., Fito, a. Andrés, Lemus, R. 2007. Mathematical modeling of hot-air drying kinetics of red bell pepper (var. Lamuyo). *Journal of Food Engineering* 79(4), 1460-1466. https://doi.org/10.1016/j.jfoodeng.2006.04.028

Waliszewski, K., Cortes, H.D., Pardio, V.T., García, M.A. (1999). Color parameter changes in banana slices during osmotic dehydration. *Drying Technology: An International Journal* 17(4-5), 955-960. http://dx.doi.org/10.1080/07373939908917583

Yagcioglu, A., Degirmencioglu, A. and Cagatay, F. 1999. Drying Characteristics of Laurel Leaves under Different Conditions. Proceedings of the 7th International Congress on Agricultural Mechanization and Energy, Adana, 26-27 May 1999, 565-569.

Yaldiz, O. and Ertekin, C. 2001. Thin Layer Solar Drying of Some Vegetables. *Drying Technology* 19, 583-597. https://doi.org/10.1081/DRT-100103936